RESEARCH PAPER

Investigation of Self-Cleaning Properties of MoO_3-rGO Nanocomposite Thin Films: Plasma Treatment Effect

Mustafa H. Saeed *, Israa Mudher Hassan, S. M. Alduwaib, Safaa Abed Salih

Department of Science, Collage of Basic Education, Mustansiriyah University, Baghdad, Iraq

ARTICLE INFO

Article History:
Received 10 June 2026
Accepted 22 September 2026
Published 01 October 2026

Keywords:
AFM
MoO_3-rGO
Nanocomposite
Self-Cleaning Properties

ABSTRACT

In this study, the synthesis of the thin layers of MoO_3 and MoO_3 - rGO nanocomposites was performed using spray pyrolysis device. The structural and morphological features of the thin layers synthesized before and after plasma treatment were studied using X Ray Diffraction (XRD), Atomic Force Microscope (AFM) and Field Emission Scanning Electron Microscope (FE-SEM). In X-ray diffraction spectrum of the samples, after plasma treatment, amorphous behavior is observed compared to before plasma. FTIR analyses were performed to determine the type of bonds formed, and the PL to characterize the photoluminescence. After plasma, adsorption also increases to some extent in the presence of reduced graphene oxide in MoO_3–rGO composite, but plasma treatment does not change the shape of the peaks and adsorption region. Investigating the self-cleaning properties of synthesized thin films shows that the degree of surface roughness has increased due to plasma treatment and accordingly, the surfaces of synthesized thin films have changed from hydrophilic to hydrophobic state.

How to cite this article
Saeed M., Hassan I., Alduwaib S., Salih S. Investigation of Self-Cleaning Properties of MoO_3-rGO Nanocomposite Thin Films: Plasma Treatment Effect. J Nanostruct, 2026; 16(4):5782-5796. DOI: 10.22052/JNS.2026.04.107

INTRODUCTION

Molybdenum oxide is a transition metal oxide that has many applications such Molybdenum oxide is a transition metal oxide that has many applications such as imaging devices, smart windows and rechargeable battery electrodes, gas sensors [1]. MoO_3 is known as one of the most widely used photocatalysts with a wide gap of 3.15eV, which its catalytic efficiency has long been known [2, 3]. Molybdenum oxide has three common phases:

The orthorhombic phase (α-MoO_3), the hexagonal phase (h-MoO_3) and the highly stable monoclinic phase (β-MoO_3). MoO_6 octahedrons are the basic building units of all MoO_3 phases. The structure of h-MoO_3 is stable up to 436°C and it converts to orthorhombic α-MoO_3 phase at this temperature. Various methods have been used by researchers to synthesize molybdenum oxide nanostructures [4, 5], such as Liquid phase deposition [1], ultrasonic-assisted synthesis [3], solution precipitation [4, 6-8], hydrothermal synthesis [9-12], solvothermal treatment [13], solution combustion [14], spray pyrolysis [15], microwave plasma process [16], and oil bath heating and sintering combination [17].

Graphene, a flat network with sp2 hybrid, has attracted the attention of researchers (has

* *Corresponding Author Email: mustafa.edbs@uomustansiriyah.edu.iq*

This work is licensed under the Creative Commons Attribution 4.0 International License.
To view a copy of this license, visit http://creativecommons.org/licenses/by/4.0/.

been considered by researchers) due to high specific surface area, high electrical conductivity, high mechanical strength and high flexibility [18-19]. Graphene is one of the newest carbon nanostructures that, a short time after its discovery and synthesis, has found many applications in various fields such as medicine, aviation Industries, oil and petrochemical industries and smart drug carrier engines [20-22]. In addition to the lower cost of synthesizing the graphene than other carbon nanostructures, it is a suitable option for using in many industries due to two-dimensional structure and more adsorption sites [23].

Yang et al. prepared the MoO_3–rGO composite using hydrothermal method, however, they did not introduce any application for this compound [24]. Noerochim et al. synthesized the rGO-MoO_3 using a two-stage hydrothermal method and used it in the manufacture of lithium batteries [25].

As mentioned above, metal oxides play an essential role in the applications of various technologies. In the study, thin films of molybdenum oxide and rGO-MoO_3 composite were synthesized by spray pyrolysis method and the plasma treatment effect on their structural, morphological, optical and self-cleaning properties was investigated.

MATERIALS AND METHODS

Graphene oxide colloid was purchased from Borhan Nanomeghyas Company, Iran. The other materials used in the research are from Merck brand.

Synthesis of Molybdenum Oxide (MoO_3)

The mixing of 0.3 g of ammonium heptamolybdate and 100 milliliter of water was done under stirring. Stirring the solution was performed for 2 hours at 50°C.

Synthesis of Reduced Graphene Oxide

Mix 300 ml of graphene oxide at 1 g/l concentration with 3 ml of ammonia and a few drops of hydrazine hydrate under stirring, and then adjust the temperature up to 100°C. The resulting solution was kept for 1 hour under stirring at this temperature.

Synthesis of the MoO_3-rGO Nanocomposite

100 ml of reduced graphene oxide solution obtained from the previous stage placed in the ultrasonic for 30 minutes. Then it was mixed with 0.3 g of ammonium heptamolybdate and stirred for 2 hours at 50°C.

Deposition by Spray Pyrolysis Method

Washing the glass substrates were performed in an ultrasonic bath for 30 minutes. MoO_3 and MoO_3-rGo solutions were sprayed onto glass slides. Spray rate of 5 ml/min and nozzle height of 30cm was selected. Carrier gas used was the compressed air. Substrate temperature was set at 120°C for all samples.

Plasma treatment

The activation of the surface of the thin layers prepared by spray pyrolysis is performed by plasma treatment and the surface roughness was created on them that prepared the surfaces for the next operation. The distance of about 4 cm was selected for the plasma head from the thin layer. The power of the plasma was 1kW, operating frequency was 20 kHz and the air was selected as the applied gas. The treated thin layers were placed in the radiant dryer at 200°C.

Characterizations

In order to investigate the formation of thin layers synthesized by spray pyrolysis method, we used the X-ray diffraction (XRD) technique, D8 Advance Bruker YT model, under CuK_α radiation. For investigating the surface morphology and chemical analysis of the synthesized layers, there was used the scanning electron microscope (FE-SEM), MIRA3 TESCAN, XMU model equipped with map and EDX analysis. In order to evaluate the surface topology of the layers, we used the images of AFM prepared by atomic force microscope (AFM) device, manufactured by Ara-Research Company. Fourier transform infrared spectrometer, Nicolet AVATAR 370 equipment model was used in the range of 400-4000 Cm^{-1} to evaluate the chemical bonds in the obtained films. Photoluminescence features were investigated using the PL device, Perkin Elmer LS 45 model. The optical adsorption spectrum from U-3500 UV/Vis device, in the 200-700 nm was used for studying the optical properties of these films. For measure the self-cleaning features of the layers, the contact angle of water droplets with 1 microliter volume on the layers of molybdenum oxide and molybdenum oxide- reduced graphene oxide composite was measured at room temperature at 25° by Dino-Lite digital camera (AM-7013 MZT model), Taiwan.

(cc) BY

RESULTS AND DISCUSSIONS

XRD Analysis

Fig. 1a shows the X-ray diffraction (XRD) pattern of MoO_3 thin films deposited by sol-gel method in the stage of before plasma. Indexing the XRD peaks at 2θ~12.82°, 25.73°, 33.66°, 35.59°, 39.16°, 46.04°, 49.21° correspond to planes (020), (040), (111), (121), (060), (200) and (002) were matched with pdf card number 00-001-0706, for confirming the formation of orthorhombic α-MoO_3 phase [26]. In addition, XRD peaks at 2θ~23.38° and 27.35° indicate the presence of a distinct secondary phase reflection from the transformed phase, which can be related to (101) and (210) planes with pdf card number 03-065-2421) [27].

Fig. 1b also shows the X-ray diffraction (XRD) pattern of the thin film of MoO_3/rGO nanocomposite in the position before plasma treatment in the range 2θ = 10-70°. In MoO_3/ rGO nanocomposite, the diffraction peaks are sharp according to (020), (040) and (060) planes, indicating the highly anisotropic growth of the angular chains of the common (shared) edges of MoO_6 octahedron with two similar chains, and creating the stoichiometric films in ac-plane MoO_3. These layers accumulate in b-axis and are joined (hold) together by VdW forces. The preferred orientation of α-MoO_3 structure shows the high crystalline nature of the synthesized samples [28, 29].

The lack of diffraction peak at 2θ=11° in spectrum of Molybdenum Oxide/ reduced graphene oxide nanocomposite shows the complete reduction of graphene oxide to reduced graphene oxide during thermal reaction procedure associated with spray pyrolysis deposition [30].

Fig. 2 shows the X-ray diffraction pattern for the thin layers of Molybdenum Oxide and Molybdenum Oxide/ reduced graphene oxide composite after plasma treatment. From the spectrum of MoO_3 thin film, the spectra have amorphous behavior before 2θ=30 after plasma. After plasma treatment, in this case, the layer consists of β-MoO_3 phase. In fact, the peaks recorded at 2θ=39.60, 53.16, 55.30, 58.94 correspond to planes (103), (004), (120) and (014) of monoclinic β-MoO_3 phase with **J**CPDS–ICDD card 01-085-2405 [31].

In X-ray diffraction spectrum of MoO_3-rGO nanocomposites, amorphous behavior is observed after plasma treatment compared to before plasma. The peak observed at 2θ=25 is a broad spectrum. Peak intensities show a sharp decrease

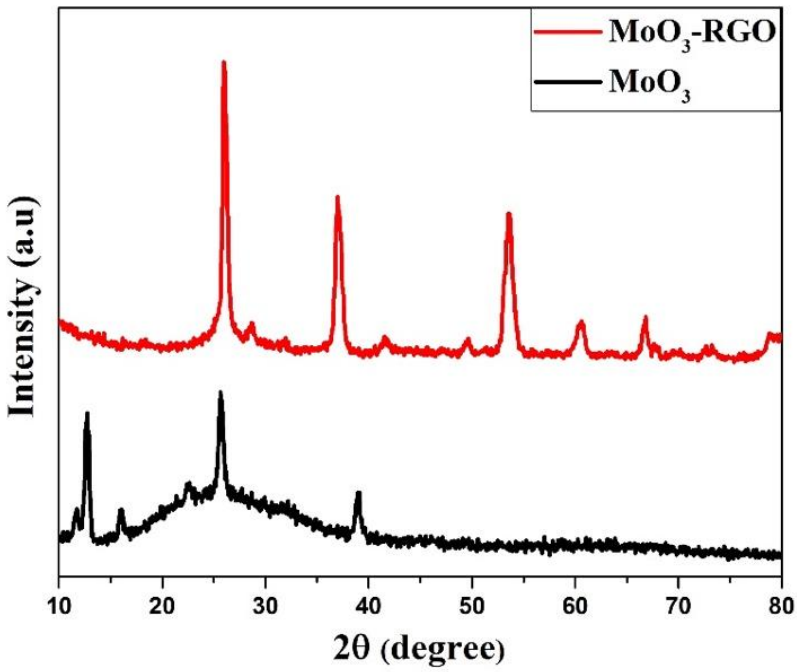


Fig. 1. X-ray Diffraction (XRD) Spectrum in Thin Layers of a) Molybdenum Oxide before Plasma, b) Molybdenum Oxide-rGO Nanocomposite before Plasma.

CC BY

compared to before plasma.

Morphological and topological properties

The morphology of MoO_3 and MoO_3–rGO nanocomposite thin films in the presence and absence of plasma were studied by field emission scanning electron microscope (FE-SEM) which is shown in Fig. 3.

As seen in Fig. 3a, the thin film of molybdenum oxide is almost uniform and consists of grains with sizes less than 25 nm. These tiny grains cling tightly to each other, creating pores inside the layer. Plasma treatment of molybdenum oxide thin films in O2 atmosphere has led to an increase in the average grain size above 40 nm and a decrease in the porosity between the grains, which is clearly seen in Fig. 3c.

MoO_3-rGO nanocomposite is composed of MoO_3 nanoparticles with a number of corrugated rGO thin sheets, that MoO_3 nanoparticles are scattered on rGO sheets. According the Fig. 4, after plasma treatment, the size of molybdenum oxide nanoparticles also increased on rGO sheets. The chemical composition of the thin layers synthesized before and after the plasma application was analyzed using Energy dispersive X-ray (EDS) spectrum and the results are shown in Fig. 4. The voltage that used to perform the tests was between zero and 10 kV. The presence of O and Mo and the lack of other elements confirm the formation of the thin film of molybdenum oxide. In the thin film of MoO_3-rGO composite, carbon element is also observed in addition to Mo and O, which indicates the presence of carbon structure of reduced graphene oxide. No changes were observed in EDS spectrum of the samples after applying the plasma.

The frequency distribution of elements in a material was showed using MAP analysis. The map results of these samples are plotted in Fig. 5, in order to evaluate the frequency distribution of molybdenum, oxygen and carbon elements in

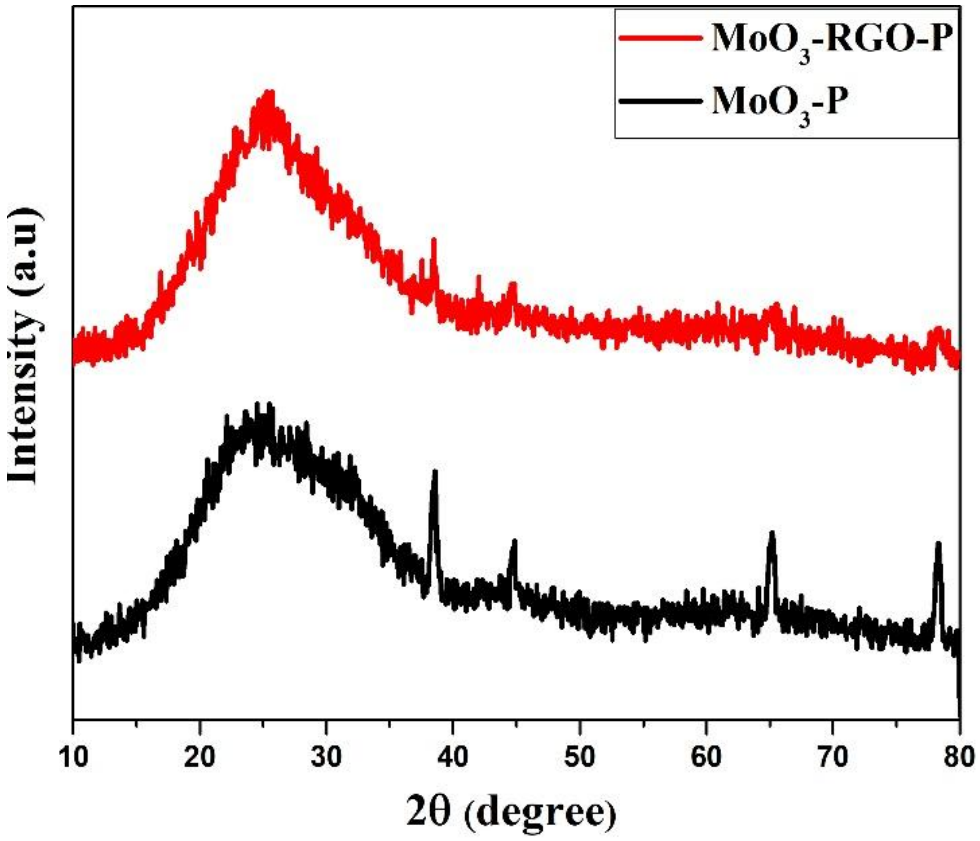


Fig. 2. X-ray Diffraction (XRD) Spectrum in Thin Layers of a) Molybdenum Oxide after Plasma, b) Molybdenum Oxide-rGO Nanocomposites after Plasma.

MoO_3 and MoO_3-rGO thin films. According to the Fig. 5, all these elements have a uniform distribution in the total surface of the prepared layers. In MoO_3 layer, only molybdenum and oxygen elements are present, and in the MoO_3-rGO composite thin film, molybdenum, oxygen and carbon elements were seen, which is consistent with EDX reports and shows the lack of impurities in the thin films.

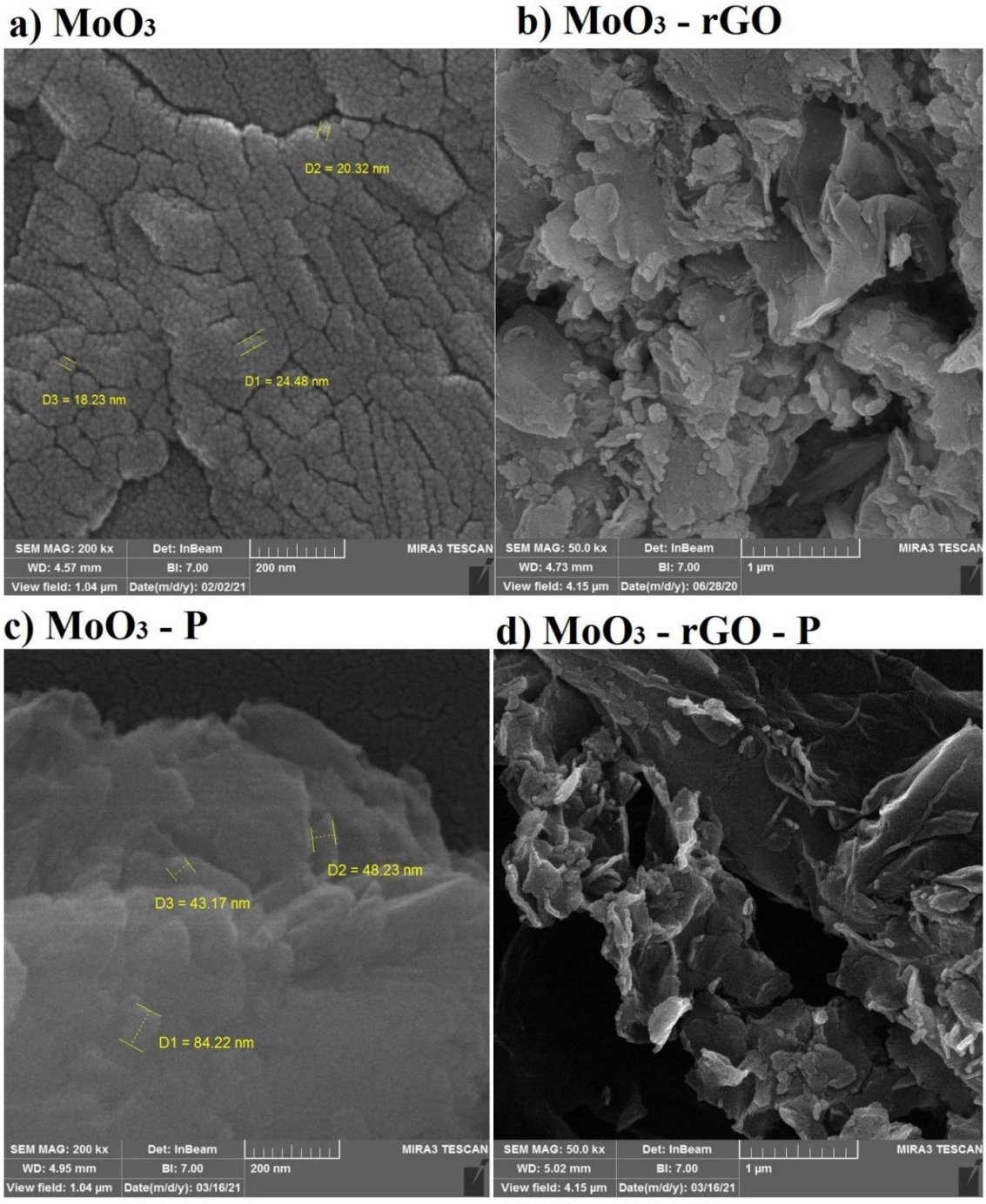


Fig. 3. FESEM pictures of Thin Layers of a) MoO3 before Applying Plasma, b) MoO_3-rGO Nanocomposite before Applying the Plasma, c) MoO_3 after Plasma, d) MoO_3-rGO Nanocomposite after Plasma.

CC BY

Figs. 6 and 7 show 2D and 3D AFM images of MoO_3 and MoO_3–rGO composites films in the presence and absence of plasma. Comparing topology image of MoO_3 and MoO_3– rGO composite thin layers, it can be seen from Fig. 6 that the surface of molybdenum oxide thin film is composed of relatively small grains, but in its composite, reduced graphene oxide plates have covered these grains. The surface is relatively smooth with slight roughness and peak-valleys.

AFM images also show that the surface morphology of the thin layers has changed after plasma treatment. Comparing Figs. 6 and 7, it can be seen that the surface of MoO_3– rGO composite thin layers without plasma treatment is almost smooth compared to after plasma treatment,

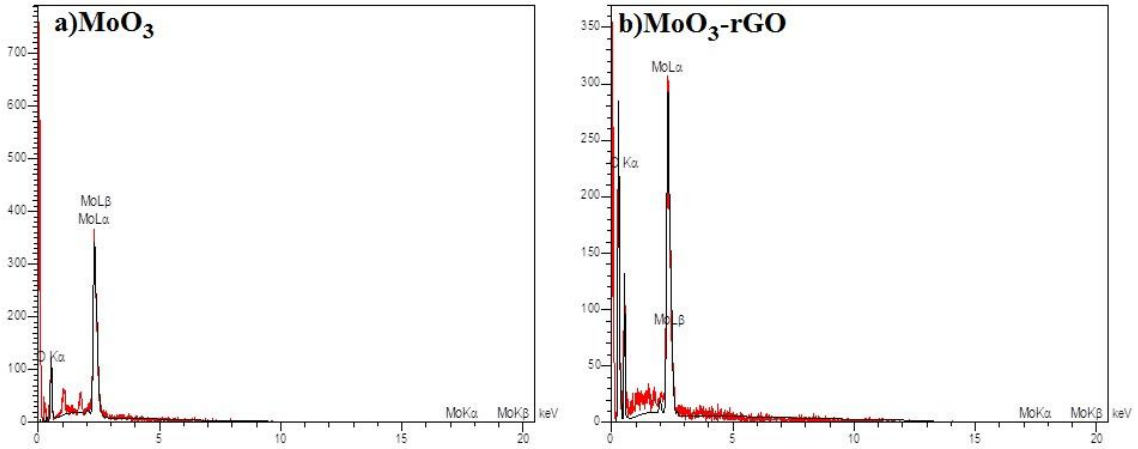


Fig. 4. Energy Dispersive X-ray Spectrum of Thin Layers of a) Molybdenum Oxide, b) Molybdenum Oxide-rGO.

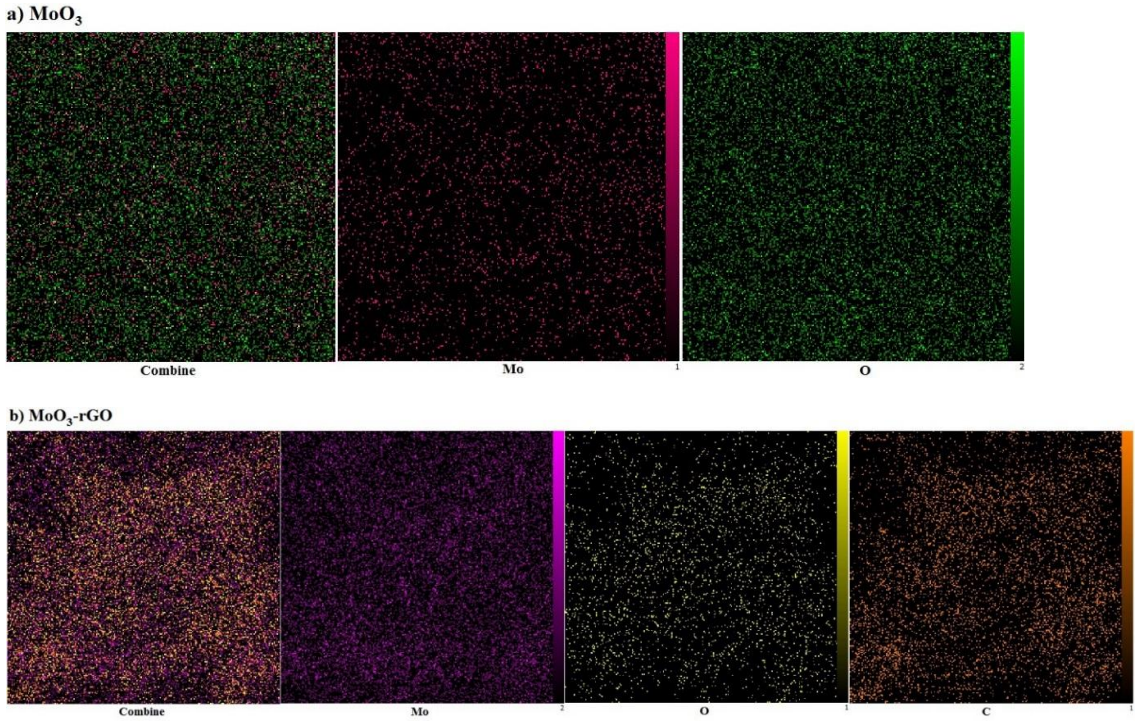


Fig. 5. Map Analysis of Thin Layers of a) Molybdenum Oxide, b) Molybdenum Oxide-rGO.

CC BY

and the slight peak and troughs is observed. After plasma treatment, the degree of surface roughness and its peak and troughs have clearly increased. It is obvious that the surface morphology of the film synthesized by spray pyrolysis method has become rougher by applying the plasma.

FTIR

Figs. 8a and 8b show the FT-IR spectrum of the thin films of MoO_3 and MoO_3– rGO composite before plasma treatment. The extreme peaks at 605, 874, and 992 cm^{-1} in IR spectrum are related to tensile mode the oxygen (O) associated with 3 metal atoms, the tensile mode of O in Mo-O-Mo units, and the tensile mode of Mo=O, respectively. The peak shown in 1610 cm^{-1} (Fig. 8b) related to C-C tensile vibrations shows the formation of reduced-GO. Meantime, the lack of a carbonyl peak at 1700 cm^{-1} shows replacement of CO by MoO_3 in the surface of reduced-GO sheets [38].

Figs. 9a and 9b show the FT-IR spectrum of the thin film of Molybdenum Oxide and Molybdenum Oxide – reduced graphene oxide composite in the 300-3800cm^{-1} after plasma treatment. In Fig. 9a, as can be seen in MoO_3 thin film, there are three strong vibrations at 621, 874 and 993 cm^{-1}, that are related to the tensile mode of oxygen associated with the three metal atoms, the tensile mode of oxygen in Mo-O-Mo units and Mo=O tensile mode of α-MoO_3 thin film with orthorhombic phase, respectively [39]. Two weak vibrations were also observed in 1384 and 1643 cm^{-1}, respectively,

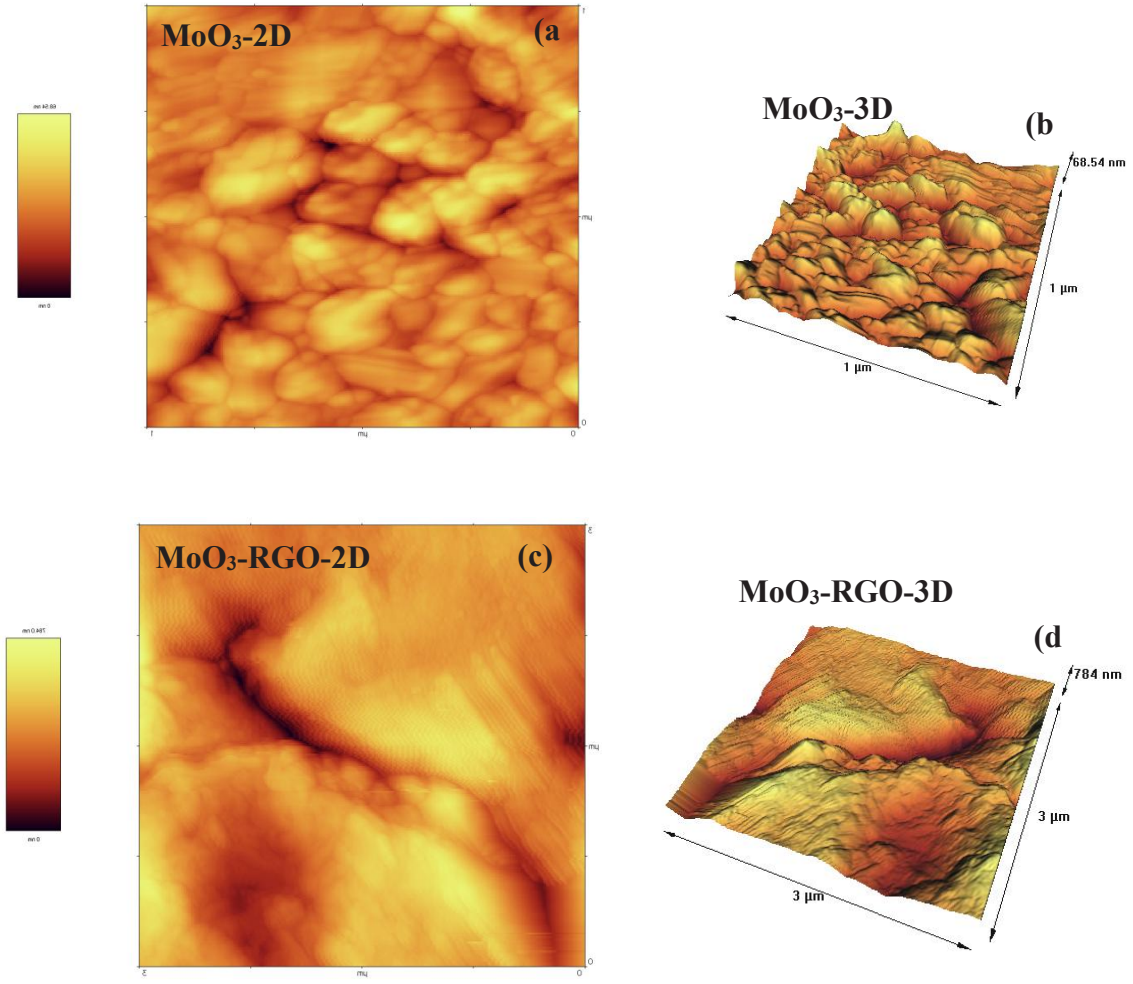


Fig. 6. a) 2D, b) 3D AFM Images of Molybdenum Oxide Thin Layer without Plasma Treatment, c) 2D and d) 3D AFM Images of the of Molybdenum Oxide- Reduced Graphene Oxide Composite Thin Layer before Plasma Treatment.

CC BY

which are related to the vibrational mode of Mo-OH band and the bending mode of absorbed water, respectively [39,40].

In FT-IR spectrum of Molybdenum Oxide–reduced graphene oxide nanocomposites, after plasma, tensile vibrational modes shifted to 870 and 990 cm^{-1} cm due to the reduction of graphene oxide. Due to the flexural vibrational mode, ~ 537 cm^{-1} band appeared in the composite material where the oxygen atom bonds to three Mo metals. In Molybdenum Oxide–reduced graphene oxide nanocomposite, the carbonyl tensile bond (C=O) disappears, which can generally be seen in about 1700 cm^{-1} because the carbonyl groups of reduced graphene oxide nanosheets were replaced by Molybdenum Oxide [41-44]. The broad adsorption band emerged in 1610 cm^{-1}, which is related to C-C tensile vibrational mode. The broad adsorption band observed in 3418 cm^{-1} is related to H-O tensile vibrational mode. This functional group is useful for hydrogen bonding between Molybdenum Oxide and reduced graphene oxide nanoplates.

Photoluminescence

Fig. 10 shows the room-temperature PL emission at the excitation wavelength of 380 nm for thin films of MoO_3 and MoO_3–rGO nanocomposites before plasma treatment. The PL spectrum in MoO_3 thin film shows emission peaks in 400-550 nm region. The emission rate at 430 nm is related to the band-to-band transition. The very fine shoulder peak observed at 512 nm

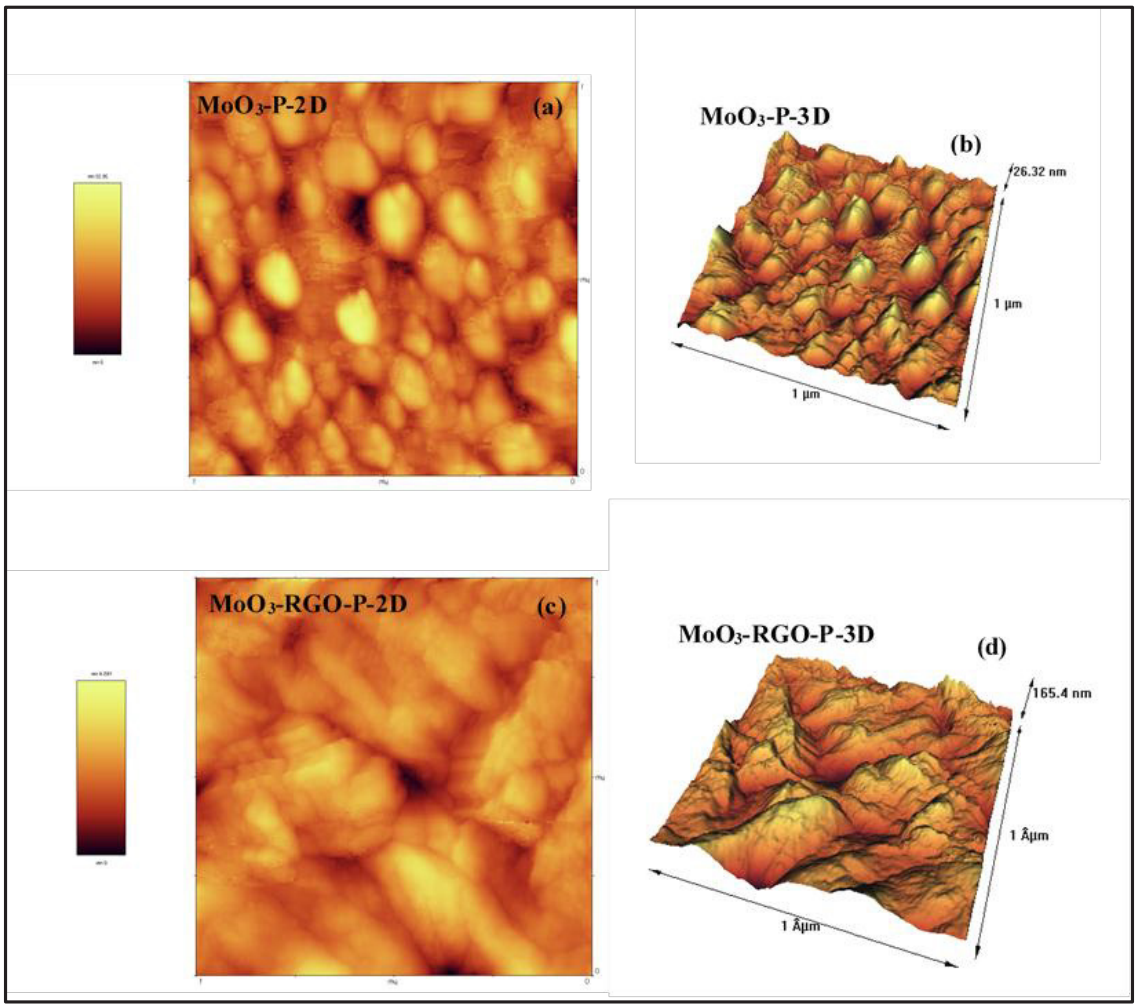


Fig. 7. a) 2D, b) 3D AFM Images of Molybdenum Oxide Thin Layer without Plasma Treatment, c) 2D and d) 3D AFM Images of Molybdenum Oxide- Reduced Graphene Oxide Composite Thin Layer after Plasma Treatment.

CC BY

is resulted from the e-h recombination between the oxygen receptors absorbed in the bottom level and conduction band [32].

In the MoO_3–rGO composite thin film, an electronic transfer from electron of conduction band to deep surfaces leads to green emission. Fig. 10a shows a wide emission with peaks located at 388, 415, 455, and 533 nm. This phenomenon indicates the simultaneous emission of all transitions from different defect states. At 3.76 eV excitation, most emissions in the region of Ultra-Violet and region blue subside, and overcomes violet emissions with weak green emissions. Subsiding the PL was seen in Molybdenum Oxide/ reduced graphene oxide composites, showing that a large number of excited electrons are transferred from the conduction band of Molybdenum Oxide to Fermi level of reduced graphene oxide [33, 34].

The PL emission was studied for α-MoO_3 thin films with plasma-treated orthorhombic phase at 380 nm excitation wavelength at ambient temperature. According to report of Song et al., the PL spectrum in Fig. 11a presents a broad peak in the range of 400-600 nm with strong indigo emission located at 430-440 nm [35]. These emissions are resulted from band-to-band transition. In this study, very weak shoulders were also identified, resulting from e-h recombination between the sublevel of the absorbed oxygen receptors and the conduction band [35].

The photoluminescence spectrum for the thin film of MoO_3–rGO composite after plasma treatment is indicated in Fig. 11b. From this Fig. 11, a main peak is seen at 453 nm. The intensity of photoluminescence peak of MoO_3–rGO shows a significant decrease as a function of reduced graphene oxide content relative to the PL peak in the spectrum of MoO_3. The result shows that the recombination velocity of excited electron holes in MoO_3 is high. But in MoO_3– reduced graphene oxide composite, the synergistic effect of the electron donor (MoO_3) and an electron receptor

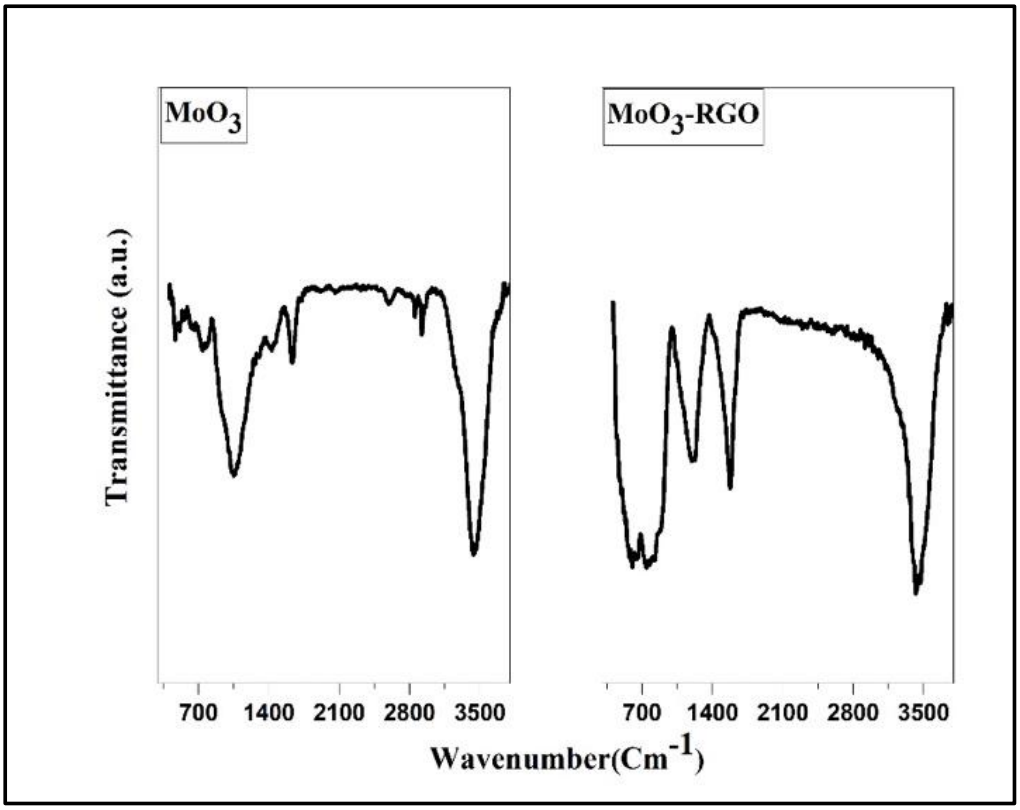


Fig. 8. FT-IR spectra of a) Molybdenum Oxide thin film, and b) Molybdenum Oxide – reduced graphene oxide nanocomposite.

CC BY

(reduced graphene oxide) reduces facilitation of electron transfer at bond line, that effectively reduces the electron-hole recombination and results to an increase in the separation of the load carrier [36-37].

Optical Adsorption (Absorption) Studies

Fig. 12a, b indicates the data form UV–Vis reflectance spectrophotometric for the thin films of Molybdenum Oxide and MoO_3– rGO composite before plasma treatment. Adsorption detected in UV wavelength region is observed at < 420 nm for α-MoO_3 thin film. This result is because of the electronic transfer between 4d electrons in the conduction band of Molybdenum and 2p electrons in the valence band of Oxygen. The adsorption edge gradually expanded up to 520 nm with the addition of rGO in MoO_3– rGO composite. This expansion of adsorption in the visible region is caused by the synergistic effect between reduced graphene oxide and Molybdenum Oxide nanostructures, that improves efficiency of electron-hole separation in MoO_3/reduced graphene oxide nanocomposites [45]. In addition, the adsorption is increased due to the insertion of Graphene Oxide, which enables light adsorption in the region with higher wavelengths.

Fig. 13a, b shows the data from UltraViolet–Visible reflectance spectrophotometric for the thin films of Molybdenum Oxide and MoO_3–rGO composite after plasma treatment. Adsorption in MoO_3 layers after plasma treatment is still in the >400 nm range and has not changed much. After plasma, adsorption also increases to some extent with the presence of reduced graphene oxide in MoO_3– rGO composite, but plasma treatment does not change the shape of the peaks and adsorption region.

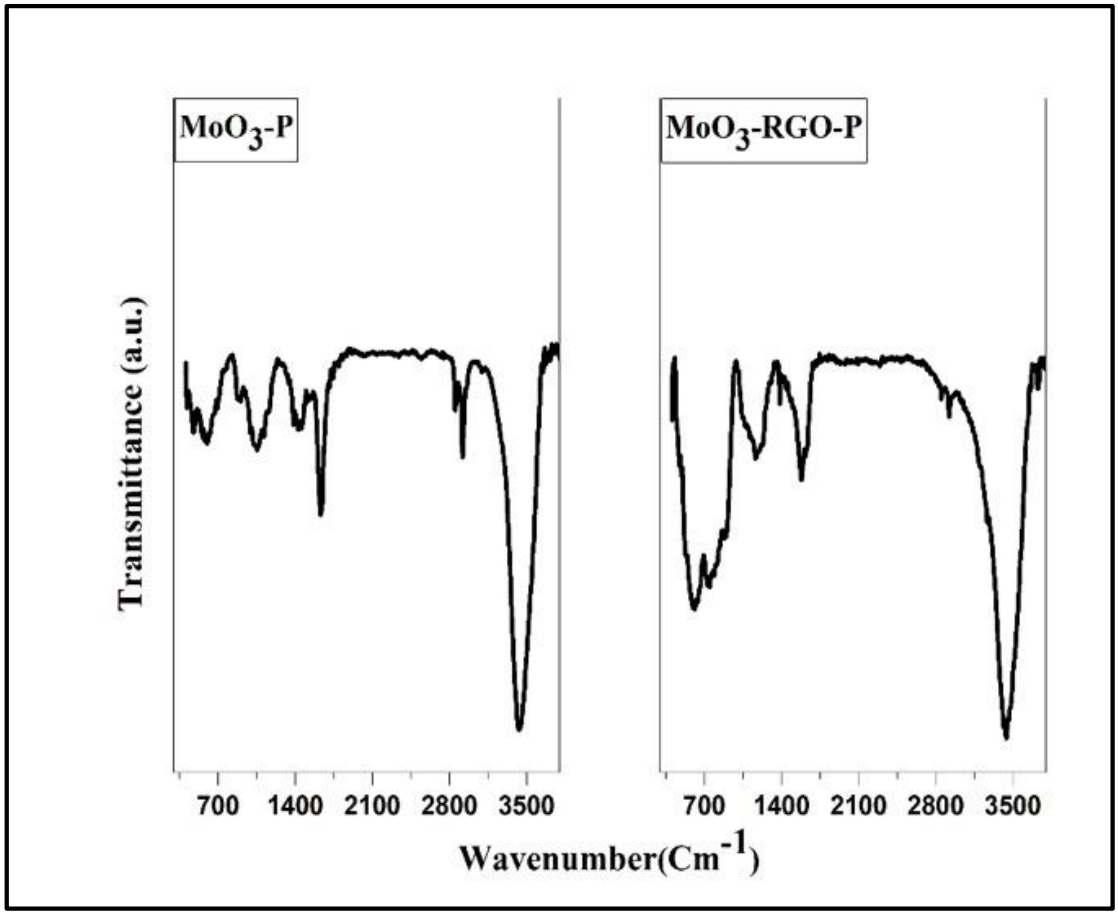


Fig. 9. FT-IR spectra of a) MoO_3 thin film after plasma, and b) MoO_3–rGO nanocomposite after plasma.

Investigating the Contact Angle

Measuring the contact angle is conducted to evaluate the interaction of the surface of the thin layer and water droplet. The contact angle (CA) parameter determined the wetting behavior of the surface. When CA is <90°, the wetting of a surface is occurred and non-wetting is happened when CA is larger than 90°, and consequently, they are

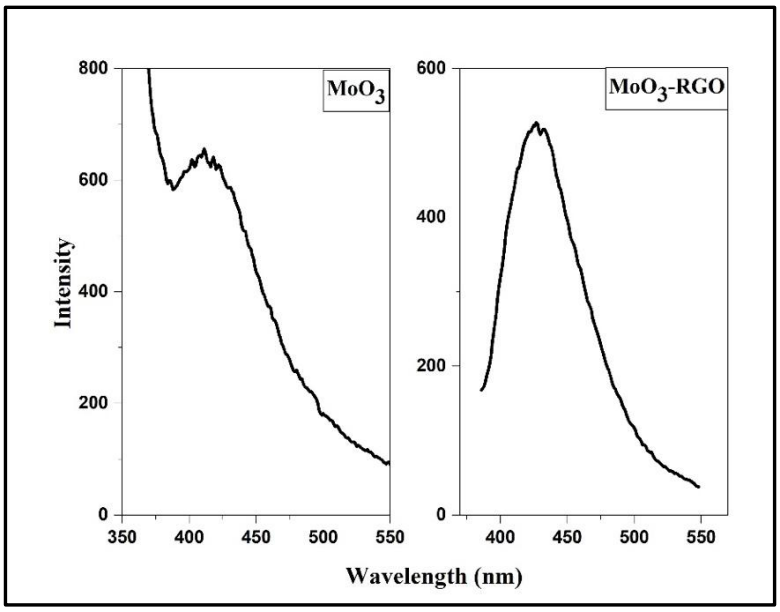


Fig. 10. Photoluminescence Spectrum of Thin Layers of a) MoO_3 before Plasma, b) MoO_3–rGO Nanocomposites

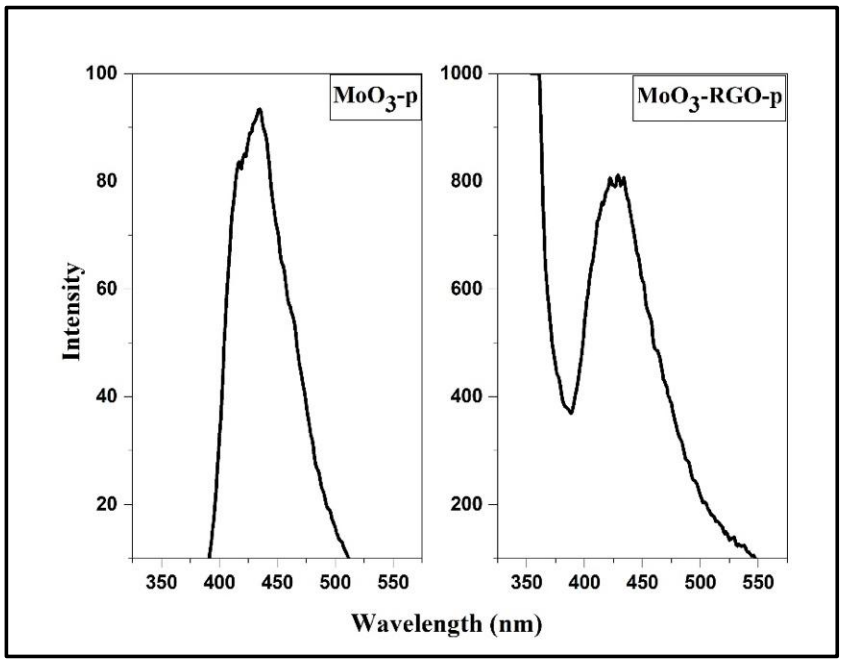


Fig. 11. Photoluminescence Spectrum for Thin Layers of (a) Molybdenum Oxide after Plasma (b) Molybdenum Oxide–rGO Nanocomposites after Plasma.

CC BY

named hydrophile and hydrophobe, respectively [41, 42].

Fig. 14 shows the shape of water droplet on the surface of thin films prepared by spray pyrolysis process in the presence and absence of plasma treatment. For investigating the self-cleaning features of the layers, water droplets with 1µl volume were placed on the thin layers of MoO_3

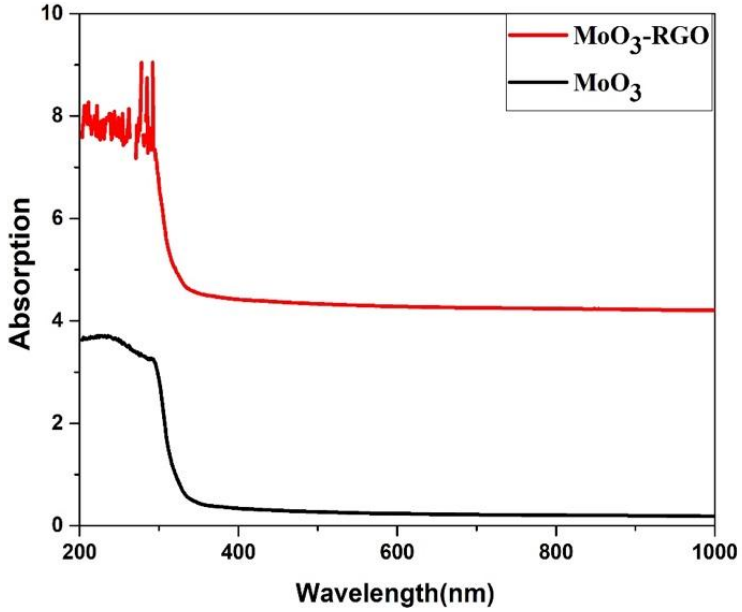


Fig. 12. UltraViolet–Visible Spectroscopy Absorbance Spectra of a) MoO_3 Thin Layer before Plasma, b) MoO_3–rGO Nanocomposite before Plasma.

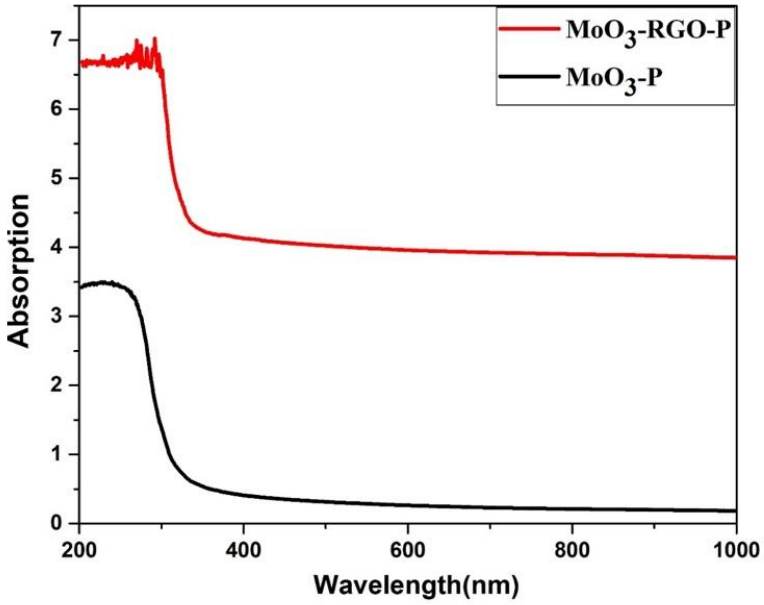


Fig. 13. UltraViolet–Visible Spectroscopy Absorbance Spectra of a) MoO_3 Thin Layer after Plasma, b) the MoO_3–rGO Nanocomposite after Plasma.

CC BY

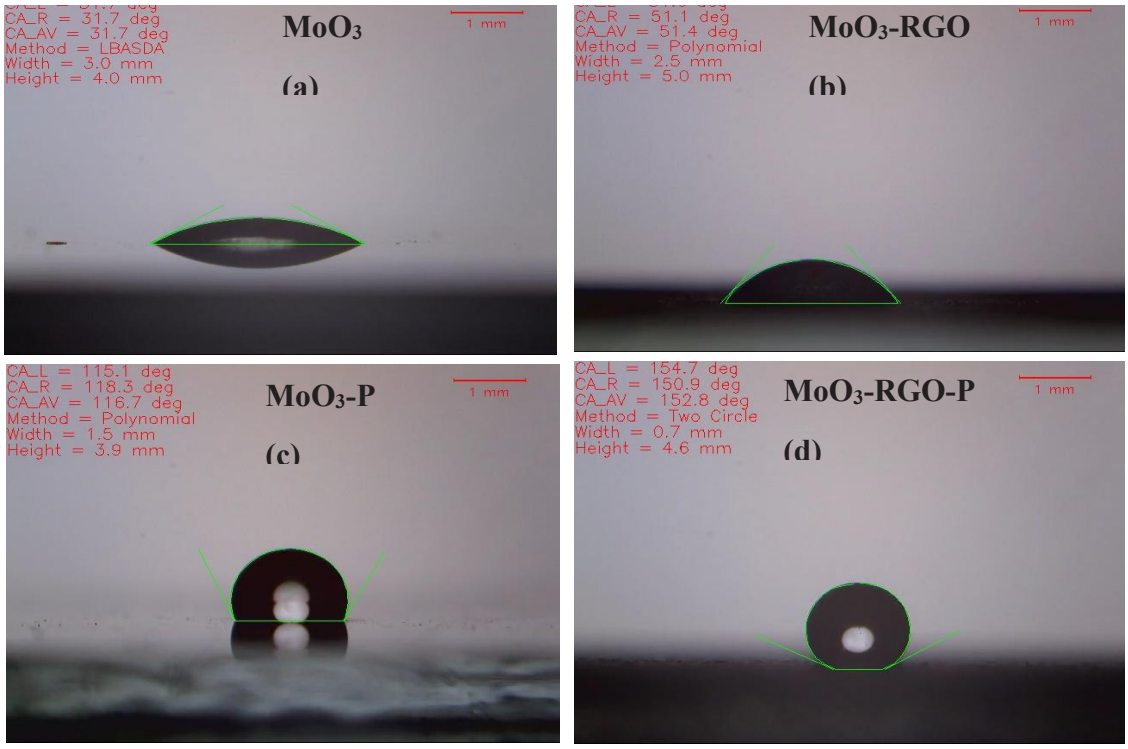


Fig. 14. The Images of Contact Angle of Thin layer of a) MoO_3 without Plasma Treatment, b) MoO_3-rGO before Plasma Treatment, c) MoO_3 after applying Plasma, d) MoO_3-rGO after applying Plasma.

and MoO_3 - rGO composite under environmental conditions. In each sample, water droplets were located in 5 various positions and its mean was considered as the contact angle.

According to the Fig. 14, MoO_3 thin film before plasma treatment has an average contact angle of 32.06 °, which shows the surface hydrophilicity of this thin film. As observed in Fig. 14c, after applying plasma, the surface of MoO_3 thin layer becomes hydrophobic and the CA of the plasma-exposed layer reaches 112.98°. The contact angle between the surface and the water droplet is influenced by two important factors: the chemical variations in surface and degree of surface roughness. According to the AFM images, it was observed that plasma treatment increases the surface roughness, therefore, it changes the surface from hydrophilicity to hydrophobicity.

Measuring contact angle between the surface and water droplet before and after plasma treatment in MoO_3-rGO thin layer is shown in Fig. 14b and 14d. As can be seen from this Fig. 14, the contact angle that droplet makes with MoO_3-rGO thin layer surface before plasma treatment is 56.8°, and as shown in Fig. 14d, after plasma treatment, the contact angle becomes 145.34°. Plasma treatment has completely changed the hydrophilic into hydrophobic behavior.

CONCLUSION

MoO_3 and MoO_3-rGO thin layers were synthesized by spray pyrolysis technique and then treated by plasma. Structural, morphological, chemical, optical and self-cleaning properties of these layers were conducted in the presence and absence of plasma treatment. XRD pattern confirmed orthorhombic phase formation of α-MoO_3. The lack of diffraction peak at 2θ=11° shows the complete reduction of Graphene Oxide to reduced GO during deposition procedure. In XRD spectrum of Molybdenum Oxide/ reduced graphene oxide nanocomposite, after plasma treatment, a broad peak is observed, which indicates the amorphous behavior of the sample. According to the results of FESEM, after plasma treatment, the size of molybdenum oxide nanoparticles has increased in the pure sample and in the nanocomposite. The chemical bonds of

CC BY

the samples were completely studied using FTIR. The optical features of the synthesized samples were examined by photoluminescence and UV-Vis spectra. The results show that the adsorption of the samples decreases to some extent after applying the plasma and in the presence of reduced graphene oxide, but plasma treatment does not change the shape of the peaks and the adsorption region. By calculating the CA between the surface and the water droplet, it is specified that contact angle increased after plasma treatment. This result is consistent with AFM images that plasma treatment has increased the degree of surface roughness. Therefore, applying the plasma changes the surface from hydrophilicity to hydrophobicity.

ACKNOWLEDGMENTS

We would like to thank Mustansiriyah University for providing the opportunity to conduct and work on this project. We also grateful for those who supported us throughout this process and our colleagues in the department of science for believing in this work.

CONFLICT OF INTEREST

The authors declare that there is no conflict of interests regarding the publication of this manuscript.

REFERENCES

1. Deki S, Béléké AB, Kotani Y, Mizuhata M. Liquid phase deposition synthesis of hexagonal molybdenum trioxide thin films. J Solid State Chem. 2009;182(9):2362-2367.
2. He T, Ma Y, Cao Y, Yin Y, Yang W, Yao J. Enhanced visible-light coloration and its mechanism of MoO_3 thin films by Au nanoparticles. Appl Surf Sci. 2001;180(3-4):336-340.
3. Du K, Fu W, Wei R, Yang H, Xu J, Chang L, et al. Ultrasonic-assisted synthesis of highly dispersed MoO_3 nanospheres using 3-mercaptopropyltrimethoxysilane. Ultrason Sonochem. 2008;15(3):233-238.
4. Jassim NM, Diwan MH, Ahmade NS. Femtosecond Optical Nonlinearity Signal and Dark Field Scattering Microscopy of Gold Coated Zinc Oxide Nanowires. Neuroquantology. 2020;18(8):66-71.
5. Bai S, Chen S, Chen L, Zhang K, Luo R, Li D, et al. Ultrasonic synthesis of MoO_3 nanorods and their gas sensing properties. Sensors Actuators B: Chem. 2012;174:51-58.
6. Wu Z, Wang D, Liang X, Sun A. Ultrasonic-assisted preparation of metastable hexagonal MoO_3 nanorods and their transformation to microbelts. Ultrason Sonochem. 2011;18(1):288-292.
7. Chithambararaj A, Bose AC. Investigation on structural, thermal, optical and sensing properties of meta-stable hexagonal MoO_3 nanocrystals of one dimensional structure. Beilstein Journal of Nanotechnology. 2011;2:585-592.
8. Al-Mgrs SSH, Al-Timimi MH, Abdullah MZ, Al-Banda WH. Structural and optical characterizations of synthesized CMC/PVP-SnO_2 nano composites. AIP Conference Proceedings: AIP Publishing; 2023. p. 090018.
9. Homad HT, Ali NM, Al-Jubouri OA, Al-Timimi MH. Synthesis and characterization of LiCo1-xNixO2 nanoparticles by urea route as cathode for lithium-ion battery. Journal of Ovonic Research. 2023;19(6):783-791.
10. Sinaim H, Ham DJ, Lee JS, Phuruangrat A, Thongtem S, Thongtem T. Free-polymer controlling morphology of α-MoO_3 nanobelts by a facile hydrothermal synthesis, their electrochemistry for hydrogen evolution reactions and optical properties. J Alloys Compd. 2012;516:172-178.
11. Alzanganawee J, Brincoveanu O, Mesterca R, Balan D, Apaz A, Enachescu M. Adhesive Properties Study of f-SWCNTs:P_3OT Nanocomposite Thin Film. ARA 40th Congress Proceedings; 2016/07/28: American Romanian Academy of Arts and Sciences; 2016.
12. Chithambararaj A, Bose AC. Hydrothermal synthesis of hexagonal and orthorhombic MoO_3 nanoparticles. J Alloys Compd. 2011;509(31):8105-8110.
13. Song J, Ni X, Zhang D, Zheng H. Fabrication and photoluminescence properties of hexagonal MoO_3 rods. Solid State Sciences. 2006;8(10):1164-1167.
14. Parviz D, Kazemeini M, Rashidi AM, Jafari Jozani K. Synthesis and characterization of MoO3 nanostructures by solution combustion method employing morphology and size control. J Nanopart Res. 2009;12(4):1509-1521.
15. Boudaoud L, Benramdane N, Desfeux R, Khelifa B, Mathieu C. Structural and optical properties of MoO_3 and V2O5 thin films prepared by Spray Pyrolysis. Catal Today. 2006;113(3-4):230-234.
16. Klinbumrung A, Thongtem T, Thongtem S. Characterization of Orthorhombic α-MoO_3 Microplates Produced by a Microwave Plasma Process. Journal of Nanomaterials. 2012;2012(1).
17. Song LX, Xia J, Dang Z, Yang J, Wang LB, Chen J. Formation, structure and physical properties of a series of α-MoO_3 nanocrystals: from 3D to 1D and 2D. CrystEngComm. 2012;14(8):2675.
18. Zhang H, Xie A, Wang C, Wang H, Shen Y, Tian X. Bifunctional Reduced Graphene Oxide/V_2O_5 Composite Hydrogel: Fabrication, High Performance as Electromagnetic Wave Absorbent and Supercapacitor. Chemphyschem. 2013;15(2):366-373.
19. Hassan NA, Albanda WH, Al-Timimi MH. Effect of ZnS and CdS on Some Physical Properties of MgO Films. East European Journal of Physics. 2023(3):296-302.
20. Fan H, Wang L, Zhao K, Li N, Shi Z, Ge Z, et al. Fabrication, Mechanical Properties, and Biocompatibility of Graphene-Reinforced Chitosan Composites. Biomacromolecules. 2010;11(9):2345-2351.
21. Cheng C, Li S, Thomas A, Kotov NA, Haag R. Functional Graphene Nanomaterials Based Architectures: Biointeractions, Fabrications, and Emerging Biological Applications. Chem Rev. 2017;117(3):1826-1914.
22. Saeed MH, Al-Timimi MH, Hussein OAA. Structural, morphological and optical characterization of nanocrystalline WO_3 thin films. Digest Journal of Nanomaterials and Biostructures. 2021;16(2):563-569.
23. Kuila T, Bose S, Mishra AK, Khanra P, Kim NH, Lee JH. Chemical functionalization of graphene and its applications. Prog Mater Sci. 2012;57(7):1061-1105.
24. Yang X, Lu C, Qin J, Zhang R, Tang H, Song H. A facile one-

CC BY

step hydrothermal method to produce graphene–MoO_3 nanorod bundle composites. Mater Lett. 2011;65(15-16):2341-2344.
25. Epifani M, Arbiol J, Díaz R, Andreu T, Siciliano P, Morante JR. Morphological and structural characterization of WO_3 and Cr–WO_3 thin films synthesized by sol–gel process. Thin Solid Films. 2010;518(16):4512-4514.
26. Hanawalt JD, Rinn HW, Frevel LK. Chemical Analysis by X-Ray Diffraction. Industrial and Engineering Chemistry Analytical Edition. 1938;10(9):457-512.
27. Andersson G, Magnéli A, Sillén LG, Rottenberg M. On the Crystal Structure of Molybdenum Trioxide. Acta Chem Scand. 1950;4:793-797.
28. Zhou J, Song J, Li H, Feng X, Huang Z, Chen S, et al. The synthesis of shape-controlled α-MoO_3 /graphene nanocomposites for high performance supercapacitors. New J Chem. 2015;39(11):8780-8786.
29. Sun Y, Wang J, Zhao B, Cai R, Ran R, Shao Z. Binder-free α-MoO_3 nanobelt electrode for lithium-ion batteries utilizing van der Waals forces for film formation and connection with current collector. Journal of Materials Chemistry A. 2013;1(15):4736.
30. Bai S, Chen C, Luo R, Chen A, Li D. Synthesis of MoO_3/ reduced graphene oxide hybrids and mechanism of enhancing H2S sensing performances. Sensors Actuators B: Chem. 2015;216:113-120.
31. Arvizu MA, Morales-Luna M, Pérez-González M, Campos-Gonzalez E, Zelaya-Angel O, Tomás SA. Influence of Thermal Annealings in Argon on the Structural and Thermochromic Properties of MoO_3 Thin Films. Int J Thermophys. 2017;38(4).
32. Ekthammathat N, Phuruangrat A, Phonkhokkong T, Maisang W, Junploy P, Klinbumrung A, et al. Sonochemical synthesis, characterization, and magnetic properties of Mn-doped ZnO nanostructures. Rare Metals. 2017;40(12):1-6.
33. Albanda WH, Fakralden DJ, Hassan NA. Enhancement in Some Physical Properties of (PVP: CMC) Blend by the addition of MgO. East European Journal of Physics. 2023(2):310-316.
34. Mondal S, Sudhu S, Bhattacharya S, Saha SK. Strain-Induced Tunable Band Gap and Morphology-Dependent Photocurrent in RGO–CdS Nanostructures. The Journal of Physical Chemistry C. 2015;119(49):27749-27758.
35. Sinaim H, Phuruangrat A, Thongtem S, Thongtem T. Synthesis and characterization of heteronanostructured Ag nanoparticles/MoO_3 nanobelts composites. Materials Chemistry and Physics. 2012;132(2-3):358-363.
36. Soliman TS, Abomostafa HM, Abouhaswa AS. Synthesis of Ni0.8Mg0.2Fe2O4 nanoparticles and its impact in enhancing the structural, magnetic, and optical properties of the PVA-CMC polymer blend. Inorg Chem Commun. 2024;164:112408.
37. Pradhan GK, Padhi DK, Parida KM. Fabrication of α-Fe_2O_3 Nanorod/RGO Composite: A Novel Hybrid Photocatalyst for Phenol Degradation. ACS Applied Materials and Interfaces. 2013;5(18):9101-9110.
38. Khandare L, Late DJ. MoO_3-rGO nanocomposites for electrochemical energy storage. Appl Surf Sci. 2017;418:2-8.
39. Zakharova GS, Täschner C, Volkov VL, Hellmann I, Klingeler R, Leonhardt A, et al. MoO_3–δ nanorods: Synthesis, characterization and magnetic properties. Solid State Sciences. 2007;9(11):1028-1032.
40. Dhanasankar M, Purushothaman KK, Muralidharan G. Effect of temperature of annealing on optical, structural and electrochromic properties of sol–gel dip coated molybdenum oxide films. Appl Surf Sci. 2011;257(6):2074-2079.
41. Bai S, Chen C, Cui M, Luo R, Chen A, Li D. Rapid synthesis of rGO–MoO_3 hybrids and mechanism of enhancing sensing performance to H_2S. RSC Advances. 2015;5(63):50783-50789.
42. Li Z, An Y, Hu Z, An N, Zhang Y, Guo B, et al. Preparation of a two-dimensional flexible MnO_2 /graphene thin film and its application in a supercapacitor. Journal of Materials Chemistry A. 2016;4(27):10618-10626.
43. Kim M, Hwang Y, Kim J. Process dependent graphene/MnO2 composites for supercapacitors. Chem Eng J. 2013;230:482-490.
44. Xia X, Hao Q, Lei W, Wang W, Wang H, Wang X. Reduced-graphene oxide/molybdenum oxide/polyaniline ternary composite for high energy density supercapacitors: Synthesis and properties. J Mater Chem. 2012;22(17):8314.
45. Kumbhakar P, Pramanik A, Biswas S, Kole AK, Sarkar R, Kumbhakar P. In-situ synthesis of rGO-ZnO nanocomposite for demonstration of sunlight driven enhanced photocatalytic and self-cleaning of organic dyes and tea stains of cotton fabrics. J Hazard Mater. 2018;360:193-203.

CC BY